Communication

Optical Excitation of a Nanoparticle Cu/p-NiO Photocathode Improves Reaction Selectivity for CO Reduction in Aqueous Electrolytes

Joseph S DuChene, Giulia Tagliabue, Alex Justine Welch, Xueqian Li, Wen-Hui Cheng, and Harry A Atwater

Nano Lett., **Just Accepted Manuscript** • DOI: 10.1021/acs.nanolett.9b04895 • Publication Date (Web): 05 Mar 2020

Optical Excitation of a Nanoparticle Cu/p-NiO Photocathode Improves Reaction Selectivity for CO_2 Reduction in Aqueous Electrolytes

*Joseph S. DuChene[†§], Giulia Tagliabue[†§], Alex J. Welch[†§], Xueqian Li[†§], Wen-Hui Cheng[†§], and Harry A. Atwater[†§]**

[†]Thomas J. Watson Laboratory of Applied Physics and [§]Joint Center for Artificial Photosynthesis, California Institute of Technology, Pasadena, California 91125 United States.

KEYWORDS artificial photosynthesis, photoelectrochemistry, hot holes, plasmonic photocathode, CO_2 reduction

Abstract

We report the light-induced modification of catalytic selectivity for photoelectrochemical CO_2 reduction in aqueous media using copper (Cu) nanoparticles dispersed onto p-type nickel oxide (p-NiO) photocathodes. Optical excitation of Cu nanoparticles generates hot electrons available for driving CO_2 reduction on the Cu surface while charge separation is accomplished by hot hole injection from the Cu nanoparticles into the underlying p-NiO support. Photoelectrochemical studies demonstrate that optical excitation of plasmonic Cu/p-NiO photocathodes imparts

increased selectivity for CO_2 reduction over hydrogen evolution in aqueous electrolytes. Specifically, we observed that plasmon-driven CO_2 reduction increased the production of carbon monoxide and formate, while simultaneously reducing the evolution of hydrogen. Our results demonstrate an optical route towards steering the selectivity of artificial photosynthetic systems with plasmon-driven photocathodes for photoelectrochemical CO_2 reduction in aqueous media.

Introduction

Artificial photosynthesis seeks to mimic the catalytic machinery of natural photosynthetic systems with inorganic materials capable of converting carbon dioxide (CO_2), water (H_2O), and sunlight into useful chemicals (e.g. ethanol, ethylene, etc.).[1-6] Unfortunately, the realization of such a process is currently hindered by catalytic challenges associated with selective conversion of CO_2 into desired products without the proliferation of unwanted side reactions.[1-6] The complexity of the reaction pathway, which involves multiple proton-coupled electron transfer steps, requires a process for preferentially activating specific chemical intermediates to reliably and selectively produce a single product of interest.[1-6] The ongoing search for selectivity has inspired numerous strategies to improve the preferential conversion of CO_2 into desired products, including nanostructuring of the electrocatalyst,[7-9] elemental alloying,[10,11] engineering of the exposed catalytic surface facets[12-15] or grain boundaries,[16-18] manipulating the local solution pH,[19-21] judicious choice of chemical additives to the electrolyte itself,[22,23] or the use of ionic liquids to limit the availability of protons.[24,25]

Despite numerous examples of improved catalyst selectivity via the aforementioned approaches, to date, the use of light as a tool for guiding the selectivity of CO_2 reduction has received considerably less attention.[26-33] Given that the most commonly used metals for

electrocatalytic CO_2 reduction, namely Ag, Au, and Cu, all support surface plasmon excitations, nanostructured metal catalysts offer new opportunities for exploiting their unique optical properties to shape the selectivity of chemical reactions.[26,34-39] In particular, the plasmon-driven production of energetic "hot" carriers on metal nanostructures has shown great promise for photocatalysis,[34-39] but the prompt decay ($t \sim 1$ ps) of hot carriers into phonon modes of the metal nanocrystal requires a strategy for quickly separating hot electron-hole pairs on an ultrafast timescale.[38,39] To that end, numerous studies have established the benefits of forming an interfacial Schottky barrier between a plasmonic metal and a wide band gap n-type semiconductor (e.g. Au/TiO_2) for separating hot carriers across the metal-semiconductor heterojunction.[40-49] Providing a channel for collecting hot electrons within the conduction band of the n-type semiconductor support effectively limits recombination processes and extends the lifetime of the charge-separated state to allow photochemistry to proceed.[47-49] Yet to promote plasmon-driven CO_2 reduction directly on the metal surface requires quickly extracting hot holes from below the metal Fermi level with a wide band gap p-type semiconductor so that hot electrons can accumulate on the metal and initiate reduction reactions with adsorbed molecules. The ability to quickly collect hot holes from metal nanostructures via charge transfer to the support also obviates the need for sacrificial reagents commonly used in plasmonic photocatalysis. Indeed, we have recently demonstrated the utility of interfacing plasmonic Au nanoparticles with p-type GaN to enable photoelectrochemical CO_2 reduction with plasmonic Au/p-GaN photocathodes.[28] Unfortunately, the limited number of p-type semiconductors suitable for such studies has hindered the development of plasmonic devices capable of harvesting hot holes from metal nanostructures for applications in photocatalysis or photodetection. Our ability to manipulate and control hot carriers from metal nanostructures is currently restricted by

insufficient knowledge of plasmon-induced hot holes; to date, relatively few experimental studies have been reported.[28,50-58]

Here, we employ p-type nickel oxide (p-NiO) as a wide band gap semiconductor support to harvest hot holes from photoexcited Cu nanoparticles and enable photoelectrochemical CO_2 reduction with plasmonic Cu/p-NiO photocathodes (Figure 1a). Nickel oxide is commonly used as a hole transport material in a variety of photovoltaic and photoelectrochemical devices due to its excellent chemical stability, high optical transparency, and suitable p-type character.[59-64] Furthermore, because p-NiO films can be deposited by a variety of low-cost methods, p-NiO may offer a more scalable option than p-type GaN as a candidate wide band gap p-type semiconductor to facilitate charge separation. In plasmonic devices, p-NiO has previously been used to collect photogenerated hot holes from Au nanoparticles, where an Ohmic contact is reportedly formed at the Au/p-NiO interface.[65-67] As a support for Cu nanoparticles, the valence band position of p-NiO (ca. −5.4 eV vs. vacuum)[60,63] relative to the Cu Fermi level (ca. −4.5 eV vs. vacuum)[68] is anticipated to establish a modest Schottky barrier (Φ_B) at the Cu/p-NiO interface that facilitates charge separation by selectively collecting plasmon-induced hot holes from the metal (Figure 1b). The large band gap of p-NiO (~3.7 eV)[63,64] ensures that any visible light incident upon the Cu/p-NiO device is incapable of directly exciting charge carriers within the p-NiO film, and it therefore serves solely to collect hot holes from the Cu nanoparticles. Furthermore, the conduction band edge of p-NiO (ca. −1.7 eV vs. vacuum)[60] relative to the Cu Fermi level provides rectification across the Cu/p-NiO interface by presenting a sizable energy barrier (~ 3 eV) to hot electron transfer at the metal-semiconductor heterojunction (Figure 1b). This plasmonic Cu/p-NiO device structure thereby limits recombination processes by providing a

pathway for hot hole collection within the underlying p-NiO film while simultaneously allowing for the accumulation of hot electrons on the Cu nanoparticles to drive CO_2 reduction.

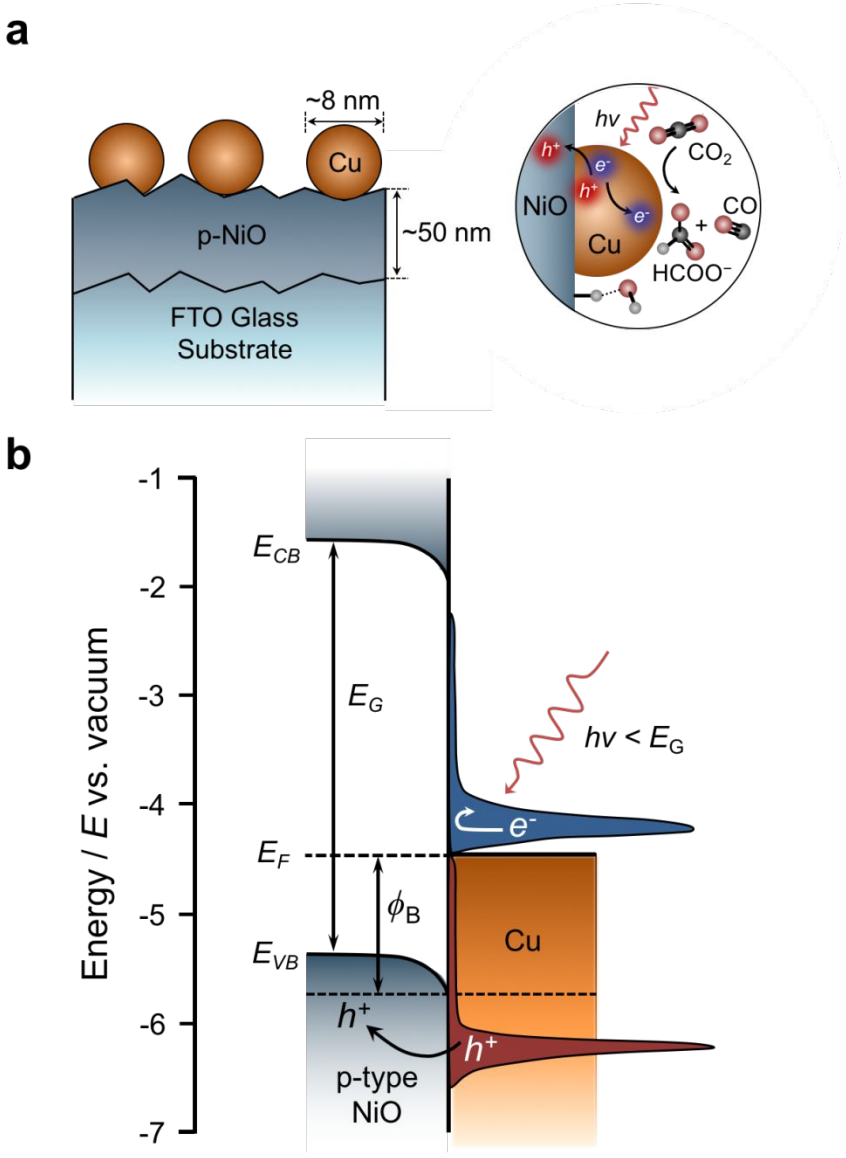

Figure 1. Plasmonic Cu/p-NiO photocathode device structure. (a) Schematic of Cu/p-NiO photocathode on fluorine-doped tin oxide (FTO) glass showing the approximate dimensions of the Cu nanoparticles (~8 nm in diameter) and the p-NiO layer (~60 nm thick) on the FTO glass substrate. (b) Predicted energy level diagram showing the relative positions of the p-NiO valence

band (E_{VB}) and conduction band (E_{CB}) relative to the Cu Fermi level (E_F). The difference in energy between the p-NiO valence band and the Cu Fermi level is expected to allow the formation of an interfacial Schottky barrier (Φ_B) to hot hole injection at the Cu/p-NiO interface of around 1 eV. Photoexcitation of Cu nanoparticles with photon energy (hv) below the band gap (E_G) of the p-NiO support generates hot electrons and hot holes on the Cu surface. The p-NiO support facilitates charge separation across the metal-semiconductor interface by allowing the collection of hot holes from the metal while also confining the hot electrons on the Cu surface to drive CO_2 reduction.

Photoelectrochemical studies of plasmonic Cu/p-NiO photocathodes confirm that visible-light excitation of Cu nanoparticles induces hot hole injection to the p-NiO valence band along with hot electron transfer to adsorbed molecules in the supporting electrolyte. The incidence of visible light was found to exert a significant influence over the selectivity of Cu nanoparticles for CO_2 reduction. Specifically, we observed that optical excitation of the Cu nanoparticles preferentially promoted the production of both carbon monoxide (CO) and formate ($HCOO^-$) while simultaneously limiting the evolution of hydrogen (H_2) in aqueous electrolytes. These results suggest that optical excitation of the metal alters the electrochemical reaction mechanism occurring on the Cu surface, with implications for the design of plasmonic photocatalysts that exhibit improved selectivity for CO_2 reduction. Overall, our studies demonstrate the utility of p-type semiconductors for the development of plasmonic photocathodes capable of artificial photosynthesis and open new possibilities for manipulating and controlling photochemistry at the nanoscale with plasmonic-metal nanostructures.

Results & Discussion

The p-NiO film was deposited onto fluorine-doped tin oxide (FTO) glass substrates via electron-beam physical vapor deposition of a metallic Ni target under flowing O_2 gas, followed by a brief heat treatment at 300 °C in ambient air to yield the desired p-type NiO phase (see Methods and Figure S1 in Supporting Information). Mott-Schottky analysis of the p-NiO film confirms that they exhibit p-type conductivity with a flat-band potential (E_{fb}) of around 0.75 V_{RHE} (V vs. RHE) and a carrier density of around 2 x 10^{19} cm^{-3} (Figure S1c). We note that these material properties of the as-synthesized p-NiO films are consistent with previous reports.[61,63] The Cu nanoparticles were subsequently formed by deposition of 3 nm of Cu directly onto the already deposited p-NiO films. No interfacial adhesion layer was used at the Cu/p-NiO heterojunction. Free from stabilizing surfactants required in colloidal nanoparticle synthesis, our approach ensures direct physical contact at the Cu/p-NiO interface while also exposing a clean Cu surface for catalysis. Scanning electron microscopy (SEM) imaging of the Cu/p-NiO device shows Cu nanoparticles distributed across the p-type NiO surface with a mean diameter d of 8 ± 2 nm (Figure 2a). Analysis of the Cu oxidation state by X-ray photoelectron spectroscopy (XPS) indicates that the as-deposited Cu nanoparticles oxidize to a mix of both Cu(I) and Cu(II) oxidation states[69] upon exposure to ambient air (Figure 2b). Further inspection of the Cu LMM region, however, strongly suggests that the oxidation state of the as-synthesized Cu nanoparticles consists of the CuO phase (Figure S2). This interpretation is further supported by the optical properties of the Cu/p-NiO films, which appear dark grey in color and display a broad peak in the visible region spanning from around 600 nm to 800 nm (Figure 2c, yellow curve). This optical response is similar to that previously observed in CuO nanoparticles.[70,71] In contrast, the bare p-NiO films are nearly transparent across the visible spectrum (Figure 2c, blue curve) and exhibit a wide band gap (E_G) of around 3.7 eV (Figure S1d).

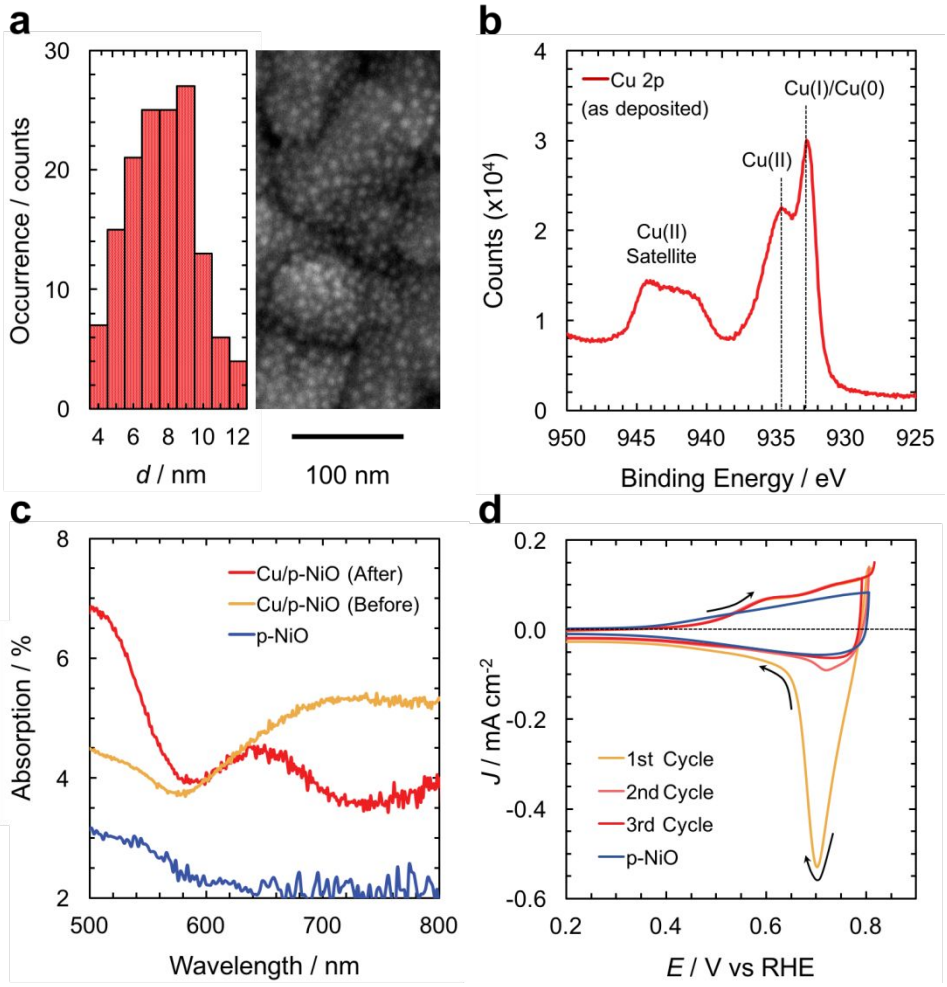

Figure 2. Materials characterization of the plasmonic Cu/p-NiO photocathode. (a) SEM image with corresponding size-distribution histogram of Cu nanoparticles (mean diameter, $d = 8 \pm 2$ nm) on a 60 nm thick p-NiO film supported on FTO glass. (b) X-ray photoelectron spectroscopy high-resolution scan of the Cu 2p region from as-synthesized Cu/p-NiO photocathodes. (c) Absorption spectra of the plasmonic Cu/p-NiO photocathode before (yellow curve) and after (red curve) electrochemical reduction via three successive cyclic voltammetry scans. The spectrum of the bare p-NiO film (blue curve) is also shown for comparison. (d) Cyclic voltammograms from

plasmonic Cu/p-NiO photocathode (yellow to red curves) and bare p-NiO films (blue curve) at a scan rate of 50 mV s^{-1}. Black arrows indicate the scan direction. The reduction of Cu oxides into metallic Cu is evidenced by the progressively smaller cathodic wave around 0.7 V_{RHE} (yellow curve) that eventually disappears after the third successive scan (red curve). A representative voltammogram from bare p-NiO films (blue curve) is shown for reference.

Photoelectrochemical studies were performed in a three-electrode configuration with the Cu/p-NiO photocathode as the working electrode, a platinum wire mesh counter electrode, and a saturated calomel electrode (SCE) as the reference electrode. The aqueous electrolyte (50 mM K_2CO_3) was sparged with CO_2 gas for 30 min prior to all electrochemical experiments, which were performed under a CO_2 blanket to prevent the ingress of atmospheric O_2 into the supporting electrolyte. All electrochemical potentials are reported with respect to the reversible hydrogen electrode (RHE). As shown in Figure 2d (yellow curve), cyclic voltammetry of the Cu/p-NiO device indicates that surface oxides formed on the Cu nanoparticles upon exposure to ambient air are successfully reduced into metallic $Cu^{(0)}$ at applied potentials more negative than 0.8 V_{RHE}. The absence of such features from bare p-NiO films (Figure 2d, blue curve) confirms that these cathodic and anodic waves are attributable to the redox features of the Cu nanoparticles. Subsequent cyclic voltammetry scans across the potential window from 0.8 V_{RHE} to 0.2 V_{RHE} indicate that any residual cupric/cuprous oxides are fully converted into metallic Cu, as evidenced by the progressively smaller reduction wave around 0.7 V_{RHE} that eventually disappears upon the third successive scan (Figure 2d, red curve). This electrochemical observation is consistent with recent *in operando* spectroscopic evidence of the electrocatalytically active phase of Cu-based cathodes.[72] We also note that a change in the

optical absorption was observed for these Cu/p-NiO films immediately after cyclic voltammetry was performed. The freshly cycled Cu/p-NiO photocathodes exhibit a new spectral feature located around 630 nm that we attribute to the surface plasmon resonance of metallic Cu nanoparticles (Figure 2c, red curve). We also observed qualitatively similar results from electrochemical reduction of Cu nanoparticle films deposited directly onto FTO glass substrates without the intervening layer of p-NiO (Figure S3). Collectively, these results strongly suggest that the oxide formed on the Cu nanoparticles upon exposure to ambient air is successfully reduced back into the metallic state under CO_2 reduction conditions.

The current-potential (*J*-*E*) behavior of the plasmonic Cu/p-NiO photocathode was assessed via linear sweep voltammetry at a scan rate of 20 mV s^{-1} under both dark conditions and visible-light excitation (λ = 565 ± 52 nm FWHM) with a high-power LED (I_0 = 160 mW cm^{-2}). As shown in Figure 3a (dotted black curve), the Cu/p-NiO device displayed a cathodic current (*J*) along the potential (*E*) sweep from 0 V_{RHE} to −1.0 V_{RHE}. The incidence of visible light (Figure 3a, solid red curve) imparts increased cathodic photocurrent (J_{ph}) relative to that observed in the dark and reduces the potential required for the onset of the Faradaic current from around −0.4 V_{RHE} in the dark to around −0.3 V_{RHE} in the light (see inset of Figure 3a). For comparison, the bare p-NiO photocathode exhibits no change in current density under visible-light excitation (Figure S4). Chronoamperometry *J*(*t*) experiments demonstrate that the plasmonic Cu/p-NiO device exhibits a prompt and reproducible cathodic photocurrent J_{ph} under periodic, visible-light illumination (λ = 565 ± 52 nm) while held potentiostatically at −0.2 V_{RHE} (Figure 3b, red curve). For comparison, no visible light response was observed from bare p-NiO supports under otherwise identical experimental conditions (Figure 3b, blue curve). The plasmonic Cu/p-NiO photocathode displays a linear J_{ph} response with respect to the incident

light power and reaches a maximum J_{ph} of around 5 μA cm^{-2} at 160 mW cm^{-2} (Figure S5). A series of high-power LEDs were also used to evaluate the incident photon-to-charge conversion efficiency [IPCE(λ)] of the Cu/p-NiO and bare p-NiO photocathodes while held potentiostatically at $E_{appl} = -0.2$ V_{RHE}. The LED power was adjusted to ensure that the same photon flux was incident on the device at each illumination wavelength (see Methods). As shown in Figure 3c, we observed that the IPCE(λ) of the Cu/p-NiO device (red points) resembled the absorption spectrum of the Cu nanoparticles (Figure 2c, red curve). The maximum IPCE of around 1.2×10^{-4} was observed with $\lambda = 565 \pm 52$ nm excitation. We emphasize that the significantly lower IPCE observed at higher photon energies strongly suggests that the photoelectrochemical activity of the Cu/p-NiO photocathode cannot be attributed to excitation of any residual Cu_2O or CuO phase. No photocurrent response was observable from the underlying p-NiO film for wavelengths longer than 505 ± 30 nm (Figure 3c, blue points).

Chronopotentiometry $V_{oc}(t)$ experiments were then performed to examine plasmon-driven charge separation across the metal-semiconductor heterojunction.[28] Hot hole injection from photo-excited Cu nanoparticles into the p-NiO film under open-circuit conditions leads to the accumulation of holes within the valence band of p-NiO. This increase of positive charge causes a shift in the V_{oc} of the Cu/p-NiO photocathode to more positive potentials relative to the equilibrium V_{oc} observed under dark conditions. Therefore, plasmon-induced hot hole transfer across the metal-semiconductor heterojunction can be observed by monitoring the influence of light on the V_{oc} of the device. Indeed, the plasmonic Cu/p-NiO device exhibits an increase in V_{oc} upon exposure to visible-light irradiation and eventually establishes a plasmonic photovoltage V_{ph} ($V_{ph} = V_{oc,light} - V_{oc,dark}$) of around 15 mV (Figure 3d, red curve). No V_{ph} response was observed from bare p-NiO films at an incident wavelength of 565 nm (Figure 3d, blue curve).

Taken together, these data are consistent with plasmon-induced hot hole injection into the p-NiO valence band along with photoelectrochemical reduction of molecular species in the supporting electrolyte.

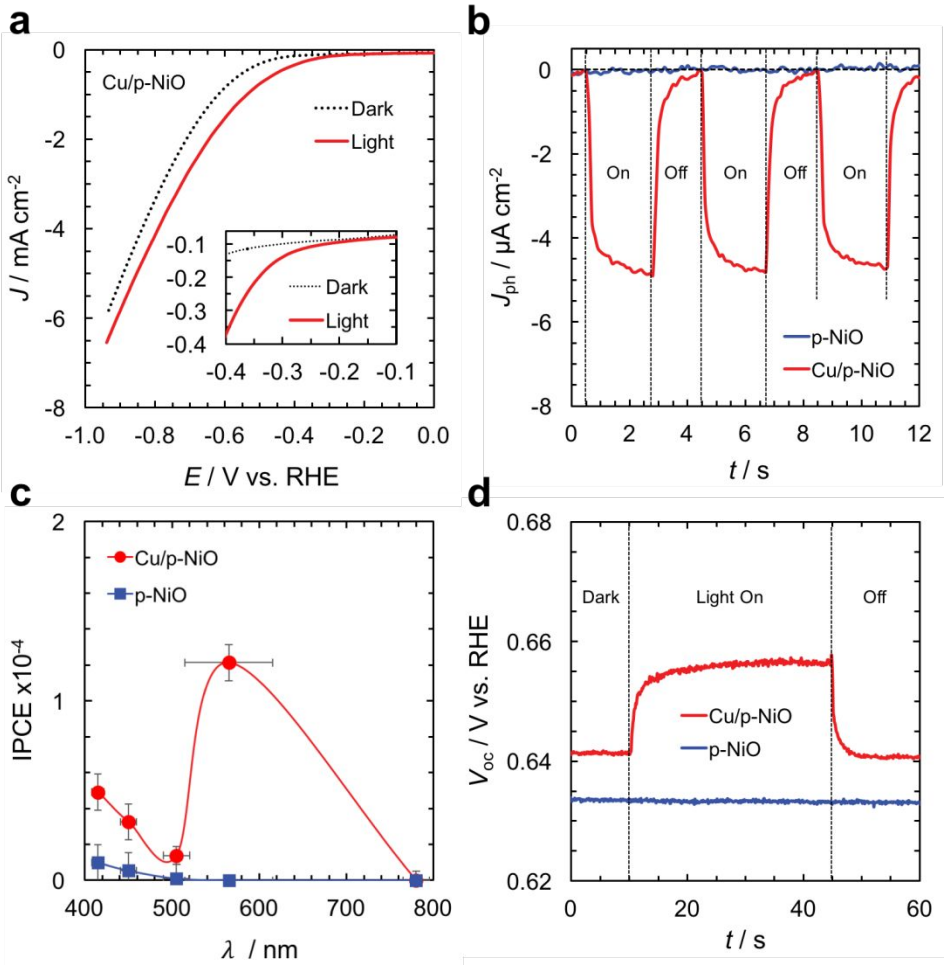

Figure 3. Photoelectrochemical characterization of plasmonic Cu/p-NiO photocathodes. (a) Linear sweep voltammetry $J(E)$ of plasmonic Cu/p-NiO photocathode at a scan rate of 20 mV s^{-1} under dark conditions (dotted black curve) and under visible-light irradiation (λ = 565 ± 52 nm) (solid red curve). (b) Chronoamperometry $J(t)$ of the photocurrent ($J_{ph} = J_{light} - J_{dark}$) obtained

from plasmonic Cu/p-NiO (red curve) and bare p-NiO (blue curve) photocathodes under periodic, visible-light irradiation (λ = 565 ± 52 nm) while potentiostatically poised at an applied potential of E_{appl} = −0.2 V_{RHE}. (c) Incident photon-to-charge conversion efficiency [IPCE(λ)] of the plasmonic Cu/p-NiO (red points) and bare p-NiO (blue points) photocathodes. The IPCE was determined by collecting the photocurrent from each device while poised at an applied potential of E_{appl} = −0.2 V_{RHE}. The IPCE error bars represent the standard deviation about the mean value and the wavelength error bars indicate the FWHM of the high-power LED. (d) Chronopotentiometry $V(t)$ of the open-circuit voltage (V_{oc}) obtained from the plasmonic Cu/p-NiO photocathode (red curve) and the bare p-NiO cathode (blue curve) under visible-light irradiation (λ = 565 ± 52 nm).

The influence of plasmon excitation on the selectivity of plasmonic Cu/p-NiO photocathodes for the CO_2 reduction reaction (CO_2RR) was then studied in a two-compartment compression cell specifically designed to enable photoelectrochemical operation.[73] Electrochemical experiments were conducted in a three-electrode configuration with the plasmonic Cu/p-NiO photocathode as the working electrode, a Pt foil as the counter electrode, and a leakless Ag/AgCl electrode as the reference electrode all immersed in a CO_2-saturated 50 mM K_2CO_3 supporting electrolyte (see Methods). Photoelectrochemical collection of hot holes from the Cu nanoparticles via the underlying p-NiO film obviates the need for sacrificial reagents. The obtained chemical products were evaluated under both dark and light (λ = 565 ± 52 nm) conditions while the plasmonic photocathode was held potentiostatically at an applied potential (E) ranging from −0.7 V_{RHE} to −0.9 V_{RHE}. The potential window available for plasmon-driven CO_2 reduction studies is restricted by the limited stability of the oxide support during

electrochemical operation at applied potentials more negative than −0.9 V_{RHE}. The gaseous and liquid products generated in the reactor headspace and electrolyte compartments were sampled and analyzed via gas chromatography and high-pressure liquid chromatography, respectively (see Methods).

As shown in Figure 4, the observed product distributions obtained under dark electrocatalysis are dependent on the applied electrochemical potential (*E*). The reported Faradaic efficiency for each chemical product represents the average value obtained from three independent trials and the error bars indicate the standard deviation. At an applied potential of *E* = −0.7 V_{RHE}, the Cu/p-NiO photocathode evolves primarily hydrogen (H_2) along with carbon monoxide (CO) and formate ($HCOO^-$) as minor products. At more negative applied potentials (*E* = −0.9 V_{RHE}), CO and $HCOO^-$ begin to comprise a more significant fraction of the total Faradaic efficiency (~40%) under dark conditions (Figure 4b-c). We emphasize that our cyclic voltammetry results (Figure 3d), together with the observed changes in the optical properties of the device (Figure 3c), indicate that the oxidation state of the Cu nanoparticles under these applied potentials is metallic $Cu^{(0)}$. This conclusion is also supported by recent *in operando* spectroscopic evidence.[72] Although a significant fraction of the products evolved from the Cu/p-NiO device consist of H_2 under dark conditions (Figure 4a, blue points), this product is largely attributable to the activity of the underlying p-NiO film that remains exposed to the electrolyte. Indeed, the bare p-NiO substrate produces almost exclusively H_2 with ~98% Faradaic efficiency across the entire potential window from −0.7 V_{RHE} to −0.9 V_{RHE} (Figure S6). The product distribution observed for the bare p-NiO control sample under CO_2RR conditions is consistent with a prior study of NiO-based cathodes.[62] We therefore assign nearly all CO_2RR products observed from the plasmonic Cu/p-NiO photocathodes to the catalytic activity of the Cu

nanoparticles (Figure S7). XPS analysis of these devices after electrochemistry indicates that the oxidation state of the Cu nanoparticles and the underlying p-NiO film is similar to that of the as-synthesized samples, suggesting that any changes associated with electrochemistry is largely reversible (Figure S8).

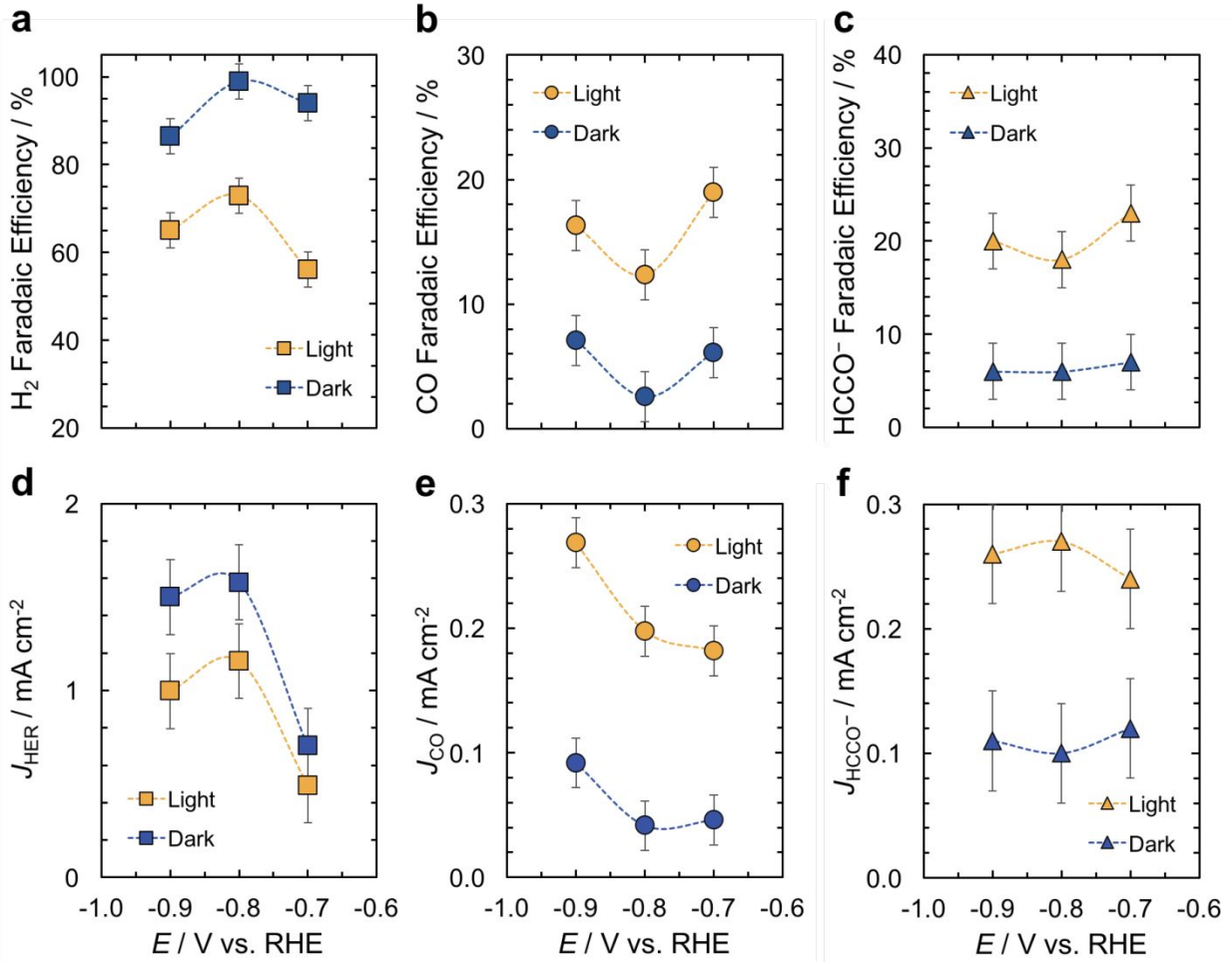

Figure 4. Distribution of CO_2 reduction products obtained from plasmonic Cu/p-NiO photocathodes as a function of the applied electrochemical potential (*E*). Faradaic efficiency (a–c) and associated partial current density (d–f) for the production of (a,d) hydrogen (H_2) (squares),

(b,e) carbon monoxide (CO) (circles), and (c,f) formate ($HCOO^-$) (triangles) during controlled potential electrolysis under dark conditions (blue symbols) and under visible-light irradiation (yellow symbols). Plasmon excitation was performed with $\lambda = 565 \pm 52$ nm at an incident power of 160 mW cm^{-2}. Data points and error bars represent the average value and standard deviation, respectively, obtained from three independent trials.

As shown in Figure 4, optical excitation of the plasmonic Cu/p-NiO photocathodes with 565 ± 52 nm light from a high-power LED ($I_0 = 160$ mW cm^{-2}) induces a marked change in the distribution of chemical products compared to that observed during dark electrocatalysis. Specifically, we observed a reduction in the Faradaic efficiency for H_2 evolution (Figure 4a, squares) concomitantly with an increase in the Faradaic efficiency for both carbon monoxide (Figure 4b, circles) and formate (Figure 4c, triangles) at all applied potentials. The biggest change in selectively was observed at -0.7 V_{RHE}, where the Faradaic efficiency for H_2 falls from nearly 94% in the dark to around 58% in the light (Figure 4a). This substantial reduction in HER activity was accompanied by a sizable improvement in the selectivity for CO_2 reduction; the Faradaic efficiency for both CO and $HCOO^-$ increased by three times relative to that observed in the dark and begin to account for nearly 50% of the total Faradaic efficiency from the device. The partial current densities associated with the H_2 evolution reaction (J_{HER}), the production of CO (J_{CO}), and the production of formate (J_{HCOO-}) are shown in Figure 4d-f, respectively. At an applied potential of $E = -0.7$ V_{RHE}, we observed little change in J_{HER} between dark and light conditions (Figure 4d), but a notable increase in both J_{CO} and J_{HCOO-} was observed (Figure 4e-f). As we moved to more negative applied potentials, the proportion of J_{CO} and J_{HCOO-} continued to increase along with a sizable reduction in J_{HER} relative to that observed during dark

electrocatalysis. At the most negative potential studied ($E = -0.9$ V_{RHE}), the J_{HER} was reduced by nearly 33% from around 1.5 mA cm^{-2} in the dark to around 1 mA cm^{-2} in the light, while both J_{CO} and J_{HCOO-} are nearly three times greater than they were in the dark. Overall, these results indicate that optical excitation of the Cu nanoparticles increases their selectivity for the CO_2RR relative to the HER at all applied potentials. We also monitored the electrolyte temperature via a thermocouple inserted within the electrochemical cell, situated near the Cu/p-NiO working electrode. Over the course of a 2 h photoelectrochemical experiment we observed a 4 °C increase in the solution temperature up to around 29 °C (Figure S9). We can exclude the possibility that increased CO_2 reduction selectivity arises solely due to plasmonic heating of the electrocatalytic surface, as it has previously been shown that increased electrolyte temperatures promote H_2 evolution while reducing the selectivity for CO_2 reduction.[73] Such heating-induced trends in reaction selectivity are clearly opposite to those observed here. The linear relationship observed between incident light power and photocurrent (Figure S5) further indicates that the improved photoelectrochemical selectivity is not associated with a thermal process. We note that these results are interesting in light of previous observations of plasmon-enhanced selectivity involving gas-phase photocatalysis conducted at elevated temperatures, in which the conversion of CO_2 and H_2 to carbon monoxide (CO) or methane (CH_4) was enhanced with optical excitation of the plasmonic photocatalyst.[29,33]

There are several possible mechanisms by which plasmon excitation of Cu nanoparticles may alter the distribution of CO_2 reduction products obtained from the plasmonic Cu/p-NiO photocathode. Here, we consider several distinct plasmon-induced processes that could account for our observed photoelectrochemical results. Photo-induced hot hole injection into the p-NiO valence band leads to increased electron density on the Cu nanoparticles, which could potentially

influence the reaction mechanism in a variety of ways. Hot electrons may be selectively injected into available molecular orbitals of adsorbed species at the metal-electrolyte interface. If such a process were to occur preferentially on adsorbed CO_2, hot electrons would selectively activate CO_2 to aid in formation of the CO_2^- species on the Cu surface. Since the initial reduction of adsorbed CO_2 is thought to comprise the rate-limiting step in CO_2 reduction,[81] the generation of hot electrons on the Cu nanoparticles via plasmon excitation may help initiate the catalytic cascade on the Cu surface by activating adsorbed CO_2 molecules.

Alternatively, it is conceivable that plasmon excitation of the Cu nanoparticles serves to reduce the evolution of H_2 from the Cu surface through a process known as desorption induced by electronic transitions (DIET).[36,37,82] In this mechanism, hot-electron transfer to adsorbed H_2 may destabilize surface bound molecules by populating anti-bonding orbitals of the adsorbate and causing the molecule to dissociate on the Cu surface prior to being released into solution. We note that it has previously been reported that plasmon-induced hot electrons can initiate photo-dissociation of H_2 molecules on metal surfaces.[74-76] As an additional consequence of molecular H_2 dissociation, surface-bound hydrogen atoms would be available to protonate nearby CO_2^- anions and facilitate CO_2 reduction. Such a process may be responsible for the suppression of H_2 observed upon optical excitation of the plasmonic Cu/p-NiO photocathode. The absence of further reduced C_2 products like ethylene, which is commonly observed in electrochemical CO_2 reduction with Cu surfaces, could also be attributed to a DIET mechanism. It is currently thought that ethylene is formed through carbon-carbon coupling via dimerization of adsorbed CO species.[2-4] If hot-electron transfer occurs preferentially to adsorbed CO molecules instead of H_2, the DIET mechanism could either initiate desorption of molecular CO from the Cu surface or photo-dissociate CO into atomic fragments. Both processes would

effectively reduce the available pool of surface-bound CO needed to form C_2 products on the metal surface.

Finally, it is possible that plasmon-induced hot hole injection to the p-NiO support modifies the molecular interactions with the Cu surface by altering the electronic structure of the Cu nanoparticles. It is well known that the electronic structure of the metal *d*-bands plays the dominant mechanism in determining molecular adsorption at a metal surface.[77,78] Although a distribution of hot holes spanning the *sp*-band down to the *d*-bands are created within the Cu nanoparticles upon visble-light excitation, direct transitions (*d*-band to *sp*-band) are the dominate mechanism for hot-hole generation when irradiated above the interband threshold of Cu (~1.6 – 1.8 eV).[79,80] Thus, optical excitation of the Cu nanoparticles with 565 nm light ($h\nu$ = 2.2 eV) preferentially excites hot holes within the metal *d*-bands[77,78] that can then transfer to the underlying p-NiO film. Injection of hot holes into the p-NiO valence band thereby alters the occupation of states below the Cu Fermi level, which could then modify the molecular surface interactions by tuning the extent of hybridization between the metal *d*-bands and the frontier orbitals of the adsorbate. This change in electronic structure of the metal via plasmon-induced hot hole transfer to the p-NiO support offers an alternative pathway towards shaping the selectivity of Cu nanoparticles.

As several reduction reactions are occurring simultaneously on the plasmonic photocathode, and both the Cu nanoparticles and the underlying p-NiO film are exposed to the electrolyte, advanced *in operando* spectroscopic studies are needed to conclusively distinguish between these possible reaction mechanisms. It is also important to recognize that the surface coverage of adsorbed molecules, along with their associated electronic structure, will influence the relative charge-transfer probabilities across the metal-molecule interface. Without *in*

operando vibrational spectroscopy it is difficult to know the identity of adsorbed species or estimate their relative surface coverage on the Cu/p-NiO surface; instead we speculate about the various species present based on our observed product distribution and what is currently known about the mechanism of electrochemical CO_2 reduction. Although the production of hydrogen (H_2), carbon monoxide (CO), and formate ($HCOO^-$) are all thought to involve two proton-coupled electron-transfer steps, these three products originate from different reactive intermediates formed on the Cu surface under reaction conditions.[2-4] The mechanism of CO_2 reduction to form CO or $HCOO^-$ is thought to proceed via two distinct intermediates formed on the Cu surface during electrochemical reduction. The evolution of CO occurs via carbon-bound *COOH intermediates while $HCOO^-$ production occurs via oxygen-bound *OCHO, where * indicates the atom bound to the surface site.[4] It therefore seems unlikely that hot electron transfer is occurring preferentially to only one of these intermediates formed on the Cu surface *in operando*, since the Faradaic efficiencies for both CO and $HCOO^-$ were observed to increase with light excitation. Instead, we suspect that plasmon-induced hot electrons on the Cu nanoparticles likely play a key role in improving the selectivity for the CO_2RR by preferentially activating CO_2 to form the CO_2^- anion. Reducing the barrier for this rate-limiting step in electrochemical CO_2 reduction[81] would be expected to increase the production of both carbon monoxide and formate. Furthermore, if a fraction of the electrochemically-derived H_2 molecules were photo-dissociated on the Cu surface by hot electrons via DIET, the surface-bound hydrogen atoms would be readily available for protonation of activated CO_2^- molecules. We also hypothesize that the injection of hot holes into the p-NiO film changes the intrinsic binding affinity of the metal surface for reactant molecules by altering the *d*-band structure of the Cu

nanoparticles. Collectively, these processes could synergistically shape the selectivity of the plasmonic Cu/p-NiO photocathode in favor of CO_2 reduction relative to the HER.

We also comment on the timescale of these potential processes in the context of the observed photochemistry. At present, it remains unclear if plasmon-induced hot electrons are transferred directly to adsorbed molecules on timescales preceding (t < 10 fs) electron-electron scattering processes (t ~ 10–100 fs) or if charge transfer occurs after establishing an excited-state Fermi-Dirac distribution at an elevated electronic temperature (t > 1 ps). Recent experimental observations[83-88] and theoretical investigations[89,90] all suggest that hot-carrier injection from a photo-excited metal nanoparticle to an adjacent phase may occur directly across the metal-molecule interface on a near-instantaneous timescale (t < 10 fs), rather than indirectly via the more traditional mechanism involving sequential processes of hot-carrier generation, thermalization, and transfer. Such a direct charge-transfer mechanism could offer a plausible explanation for the observed change in chemical selectivity via low-intensity light, as this pathway transfers energy to adsorbed molecules prior to hot-carrier decay pathways occurring in the metal itself. Direct experimental verification of the mechanism is challenging due to the ultrafast timescales (t < 10 fs) on which these charge-transfer events would occur.[87,88] Nevertheless, these initial photoelectrochemical observations indicate that optical excitation of the Cu nanoparticles alters the selectivity of CO_2 reduction relative to traditional electrochemical reduction performed under dark conditions.

In summary, we have demonstrated the benefits of using p-type NiO as a wide band gap support for harvesting hot holes from Cu nanoparticles to allow the accumulation of hot electrons on the metal surface to drive CO_2 reduction with plasmonic Cu/p-NiO photocathodes. The collection of hot holes from the Cu nanoparticles via injection to the p-NiO support also removes

the requirements for sacrificial reagents commonly employed in plasmon-induced photochemical reactions. The Cu/p-type semiconductor Schottky junction design therefore represents a path forward for the realization of plasmon-driven photocathodes capable of harnessing surface plasmon excitations to steer the selectivity of Cu surfaces for photoelectrochemical CO_2 reduction in aqueous media. We observed that plasmon excitation of the Cu nanoparticles modulates the chemical selectivity for CO_2 reduction products, increasing CO evolution and $HCOO^-$ production while simultaneously suppressing H_2 evolution. Several possible reaction mechanisms are proposed to account for the observed influence of light on the selectivity of photoelectrochemical CO_2 reduction. Although a conclusive assignment of the reaction mechanism requires *in operando* spectroscopy to observe the molecular details of the reaction occurring on the plasmonic photocathode, we speculate that plasmon-induced hot electrons likely play a key role in altering the selectivity of the reaction. Overall, our photoelectrochemical results illustrate a promising strategy towards optically manipulating the catalytic selectivity of Cu surfaces for CO_2 conversion.

ASSOCIATED CONTENT

Supporting Information.

The following files are available free of charge.

Detailed experimental methods, optical properties of bare p-NiO films and Cu nanoparticles, cyclic voltammograms of bare p-NiO photocathodes, materials characterization of p-NiO films, electrochemical CO_2 reduction with bare p-NiO photocathodes, XPS characterization of

photocathodes after electrocatalytic testing, measurements of solution temperature during photoelectrocatalysis (PDF).

AUTHOR INFORMATION

Corresponding Author

*Email: haa@caltech.edu

ORCID

Joseph S. DuChene: 0000-0002-7145-323X

Wen-Hui Cheng: 0000-0003-3233-4606

Harry A. Atwater: 0000-0001-9435-0201

Author Contributions

J.S.D. and H.A.A. conceived the idea, designed the experiments, and wrote the manuscript. J.S.D. performed all photoelectrochemical experiments with assistance from A.J.W. and X.L. J.S.D., G.T., A.J.W., and X.L. fabricated and characterized devices. W.-H.C. performed optical characterization of materials and assisted with calibration and maintenance of gas chromatography equipment. H.A.A. supervised the project. All authors have given approval to the final version of the manuscript.

Notes

The authors declare no competing financial interests.

ACKNOWLEDGMENT

This material is based upon work performed by the Joint Center for Artificial Photosynthesis, a DOE Energy Innovation Hub, supported through the Office of Science of the U.S. Department of

Energy under Award No. DE-SC0004993. G.T. acknowledges support from the Swiss National Science Foundation through the Early Postdoc Mobility Fellowship, grant n. P2EZP2_159101 and the Advanced Mobility Fellowship, grant n. P300P2_171417. A.J.W. acknowledges support from the Resnick Sustainability Institute at the California Institute of Technology and the National Science Foundation (NSF) Graduate Research Fellowship Program under Base Award No. 1745301. We thank Professor Brian McCloskey for sharing the design of the photoelectrochemical cell for temperature-controlled CO_2 reduction experiments. We also thank Dr. Matthias Richter for XPS characterization of p-type NiO and Cu/p-NiO films, which was performed at the Molecular Materials Research Center in the Beckman Institute of the California Institute of Technology.

REFERENCES

(1) Montoya, J. H.; Seitz, L. C.; Chakthranont, P.; Vojvodic, A.; Jaramillo, T. F.; Nørskov, J. K. Materials for Solar Fuels and Chemicals. *Nat. Mater.* **2017**, *16*, 70-81.

(2) Nitopi, S.; Bertheussen, E.; Scott, S. B.; Liu, X.; Engstfeld, A. K.; Horch, S.; Seger, B.; Stephens, I. E. L.; Chan, K.; Hahn, C.; Nørskov, J. K.; Jaramillo, T. F.; Chorkendorff, I. Progress and Perspectives of Electrochemical CO_2 Reduction on Copper in Aqueous Electrolyte. *Chem. Rev.* **2019**, *119*, 7610-7672.

(3) Birdja, Y. Y.; Pérez-Gallent, E.; Figueiredo, M. C.; Göttle, A. J.; Calle-Vallejo, F.; Koper, M. T. M. Advances and Challenges in Understanding the Electrocatalytic Conversion of Carbon Dioxide to Fuels. *Nat. Energy* **2019**, *4*, 732-745.

(4) Todorova, T. K.; Schreiber, M. W.; Fontecave, M. Mechanistic Understanding of CO_2 Reduction Reaction (CO_2RR) Toward Multicarbon Products by Heterogeneous Copper-Based Catalysts. *ACS Catal.* **2020**, *10*, 1754-1768.

(5) Xu, S.; Carter, E. A. Theoretical Insights into Heterogeneous (Photo)electrochemical CO_2 Reduction. *Chem. Rev.* **2019**, *119*, 6631-6669.

(6) White, J. L.; Baruch, M. F.; Pander III, J. E.; Hu, Y.; Fortmeyer, I. C.; Park, J. E.; Zhang, T.; Liao, K.; Gu, J.; Yan, Y.; Shaw, T. W.; Ebelev, E.; Bocarsly, A. B. Light-Driven Heterogeneous Reduction of Carbon Dioxide: Photocatalysts and Photoelectrodes. *Chem. Rev.* **2015**, *115,* 12888-12935.

(7) Liu, M.; Pang, Y.; Zhang, B.; De Luna, P.; Voznyy, O.; Xu, J.; Zheng, X.; Dinh, C.-T.; Fan, F.; Cao, C.; García de Arquer, F. P.; Safaei, T. S.; Mepham, A.; Klinkova, A.; Kumacheva, E.; Filleter, T.; Sinton, D.; Kelley, S. O.; Sargent, E. H. Enhanced Electrocatalytic CO_2 Reduction via Field-Induced Reagent Concentration. *Nature* **2016**, *537*, 382-386.

(8) Safaei, T. S.; Mepham, A.; Zheng, X.; Pang, Y.; Dinh, C.-T.; Liu, M..; Sinton, D.; Kelley, S. O.; Sargent, E. H. High-Density Nanosharp Microstructures Enable Efficient CO_2 Electroreduction. *Nano Lett.* **2016**, *16*, 7224-7228.

(9) De Luna, P.; Quintero-Bermudez, R.; Dinh, C.-T.; Ross, M. B.; Bushuyev, O. S.; Todorovic, P.; Regier, T.; Kelly, S. O.; Yang, P.; Sargent, E. H. Catalyst Electro-Redeposition Controls Morphology and Oxidation State for Selective Carbon Dioxide Reduction. *Nat. Catal.* **2018**, *1*, 103-110.

(10) Kim, D.; Resasco, J.; Yu, Y.; Asiri, A. M.; Yang, P. Synergistic Geometric and Electronic Effects for Electrochemical Reduction of Carbon Dioxide Using Gold–Copper Bimetallic Nanoparticles. *Nat. Commun.* **2014**, *5*, 4948.

(11) Kim, D.; Xie, C.; Becknell, N.; Yu, Y.; Karamad, M.; Chan, K.; Crumin, E. J.; Nørskov, J. K.; Yang, P. Electrochemical Activation of CO_2 through Atomic Ordering Transformations of AuCu Nanoparticles. *J. Am Chem. Soc.* **2017**, *139*, 8329-8336.

(12) Hahn, C.; Hatsukade, T.; Kim, Y.-G.; Vailionis, A.; Baricuatro, J. H.; Higgins, D. C.; Nitopi, S. A.; Soriaga, M. P.; Jaramillo, T. F. Engineering Cu Surfaces for the Electrocatalytic Conversion of CO_2: Controlling Selectivity Toward Oxygenates and Hydrocarbons. *Proc. Natl. Acad. Sci.* **2017**, *114*, 5918-5923.

(13) Lu, Q.; Rosen, J.; Zhou, Y.; Hutchings, G. S.; Kimmel, Y. C.; Chen, J. G.; Jiao, F. A Selective and Efficient Electrocatalyst for Carbon Dioxide Reduction. *Nat. Commun.* **2014**, *5*, 3242.

(14) Zhu, W.; Zhang, Y.-J.; Zhang, H.; Lv, H.; Li, Q.; Michalsky, R.; Peterson, A. A.; Sun, S. Active and Selective Conversion of CO_2 to CO on Ultrathin Au Nanowires. *J. Am. Chem. Soc.* **2014**, *136*, 16132-16135.

(15) Zhu, W.; Michalsky, R.; Metin, Ö.; Lv, H.; Guo, S.; Wright, C. J.; Sun, X.; Peterson, A. A.; Sun, S. Monodisperse Au Nanoparticles for Selective Electrocatalytic Reduction of CO_2 to CO. *J. Am. Chem. Soc.* **2013**, *135*, 16833-16836.

(16) Mariano, R. G.; McKelvey, K.; White, H. S.; Kanan, M. W. Selective Increase in CO_2 Electroreduction Activity at Grain-Boundary Surface Terminations. *Science* **2017**, *358*, 1187-1192.

(17) Feng, X.; Jiang, K.; Fan, S.; Kanan, M. W. A Direct Grain-Boundary-Activity Correlation for CO Electroreduction on Cu Nanoparticles. *ACS Cent. Sci.* **2016**, *2*, 169-174.

(18) Feng, X.; Jiang, K.; Fan, S.; Kanan, M. W. Grain-Boundary-Dependent CO_2 Electroreduction Activity. *J. Am. Chem. Soc.* **2015**, *137*, 4606-4609.

(19) Hall, A. S.; Yoon, Y.; Wuttig, A.; Surendranath, Y. Mesostructure-Induced Selectivity in CO_2 Reduction Catalysis. *J. Am. Chem. Soc.* **2015**, *137*, 14834-14837.

(20) Yoon, Y.; Hall, A. S.; Surendranath, Y. Tuning of Silver Catalyst Mesostructure Promotes Selective Carbon Dioxide Conversion into Fuels. *Angew. Chem. Int Ed.* **2016**, *55*, 15282-15286.

(21) Welch, A. J.; DuChene, J. S.; Tagliabue, G.; Davoyan, A.; Cheng, W.-H.; Atwater, H. A. Nanoporous Gold as a Highly Selective and Active Carbon Dioxide Reduction Catalyst. *ACS Appl. Energy Lett.* **2019**, *2*, 164-170.

(22) Cao, Z.; Kim, D.; Hong, D.; Yu, Y.; Xu, J.; Lin, S.; Wen, X.; Nichols, E. M.; Jeong, K.; Reimer, J. A.; Yang, P.; Chang, C. J. A Molecular Surface Functionalization Approach to Tuning Nanoparticle Electrocatalysts for Carbon Dioxide Reduction. *J. Am. Chem. Soc.* **2016**, *138*, 8120-8125.

(23) Han, Z.; Kortlever, R.; Chen, H.-Y.; Peters, J. C.; Agapie, T. CO_2 Reduction Selective for $C_{\geq 2}$ Products on Polycrystalline Copper with N-Substituted Pyridinium Additives. *ACS Cent. Sci.* **2017**, *3*, 853-859.

(24) Rosen, B. A.; Salehi-Khojin, A.; Thorson, M. R.; Zhu, W.; Whipple, D. T.; Kenis, P. J. A.; Masel, R. I. Ionic Liquid–Mediated Selective Conversion of CO_2 to CO at Low Overpotentials. *Science* **2011**, *334*, 643-644.

(25) Asadi, M. Ki, K.; Liu, C.; Addepalli, A. V.; Abbasi, P.; Yasaei, P.; Phillips, P.; Behranginia, A.; Cerrato, J. M.; Haasch, R.; Zapol, P.; Kumar, B.; Klie, R. F.; Abiade, J.;

Curtiss, L. A.; Salehi-Khojin, A. Nanostructured Transition Metal Dichalcogenide Electrocatalysts for CO_2 Reduction in Ionic Liquid. *Science* **2016**, *353*, 467-470.

(26) Yu, S.; Wilson, A. J.; Kumari, G.; Zhang, X.; Jain, P. K. Opportunities and Challenges of Solar-Energy-Driven Carbon Dioxide to Fuel Conversion with Plasmonic Catalysts. *ACS Energy Lett.* **2017**, *2*, 2058-2070.

(27) Creel, E. B.; Corson, E. R.; Eichhorn, J.; Kostecki, R.; Urban, J. J.; McCloskey, B. D. Directing Selectivity of Electrochemical Carbon Dioxide Reduction Using Plasmonics. *ACS Energy Lett.* **2019**, *4*, 1098-1105.

(28) DuChene, J. S.; Tagliabue, G.; Welch, A. J.; Cheng, W.-H.; Atwater, H. A. Hot Hole Collection and Photoelectrochemical CO_2 Reduction with Plasmonic Au/p-GaN Photocathodes. *Nano Lett.* **2018**, *18*, 2545-2550.

(29) Zhang, X.; Li, X.; Zhang, D.; Su, N. Q.; Yang, W.; Everitt, H. O.; Liu, J. Product Selectivity in Plasmonic Photocatalysis for Carbon Dioxide Hydrogenation. *Nat. Commun.* **2017**, *8*, 14542.

(30) Yu, S.; Jain, P. K. Plasmonic Photosynthesis of C_1–C_3 Hydrocarbons from Carbon Dioxide Assisted by an Ionic Liquid. *Nat. Commun.* **2019**, *10*, 2022.

(31) Yu, S.; Wilson, A. J.; Heo, J.; Jain, P. K. Plasmonic Control of Multi-Electron Transfer and C–C Coupling in Visible-Light-Driven CO_2 Reduction on Au Nanoparticles. *Nano Lett.* **2018**, *18*, 2189-2194.

(32) Yu, S.; Jain, P. K. Selective Branching of Plasmonic Photosynthesis into Hydrocarbon Production and Hydrogen Generation. *ACS Energy Lett.* **2019**, *4*, 2295-2300.

(33) Robatjazi, H.; Zhao, H.; Swearer, D. F.; Hogan, N. J.; Zhou, L.; Alabastri, A.; McClain, M. J.; Nordlander, P.; Halas, N. J. Plasmon-Induced Selective Carbon Dioxide Conversion

on Earth-Abundant Aluminum-Cuprous Oxide Antenna-Reactor Nanoparticles. *Nat. Commun*. **2017**, 8, 27.

(34) Linic, S.; Christopher, P.; Ingram, D. B. Plasmonic-Metal Nanostructures for Efficient Conversion of Solar to Chemical Energy. *Nat. Mater.* **2011**, *10*, 911-921.

(35) Brongersma, M. L.; Halas, N. J.; Nordlander, P. Plasmon-Induced Hot Carrier Science and Technology. *Nat. Nanotechnol.* **2015**, *10*, 25-34.

(36) Christopher, P.; Moskovits, M. Hot Charge Carrier Transmission from Plasmonic Nanostructures. *Annu. Rev. Phys. Chem.* **2017**, *68*, 379-398.

(37) Linic, S.; Aslam, U.; Boerigter, C.; Morabito, M. Photochemical Transformations on Plasmonic Metal Nanoparticles. *Nat. Mater.* **2015**, *14*, 567-576.

(38) Hartland, G. V.; Besteiro, L. V.; Johns, P.; Govorov, A. O. What's so Hot about Electrons in Metal Nanoparticles? *ACS Energy Lett.* **2017**, *2*, 1641-1653.

(39) Zhang, Y.; He, S.; Guo, W.; Huang, J.; Mulcahy, J. R.; Wei, W. D. Surface-Plasmon-Driven Hot Electron Photochemistry. *Chem. Rev.* **2018**, *118*, 2927-2954.

(40) Knight, M. W.; Sobhani, H.; Nordlander, P.; Halas, N. J. Photodetection with Active Optical Antennas. *Science* **2011**, *332*, 702-704.

(41) Zheng, B. Y.; Zhao, H.; Manjavacas, A.; McClain, M.; Nordlander, P.; Halas, N. J. Distinguishing Between Plasmon-Induced and Photoexcited Carriers in a Device Geometry. *Nat. Commun.* **2015**, *6*, 7797.

(42) Li, W.; Valentine, J. Metamaterial Perfect Absorber Based Hot Electron Photodetection. *Nano Lett.* **2014**, *14*, 3510-3514.

(43) Tagliabue, G.; Jermyn, A. S.; Sundararaman, R.; Welch, A. J.; DuChene, J. S.; Pala, R.; Davoyan, A. R.; Narang, P.; Atwater, H. A. Quantifying the Role of Surface Plasmon Excitation and Hot Carrier Transport in Plasmonic Devices. *Nat. Commun.* **2018**, *9*, 3394.

(44) Mubeen, S.; Lee, J.; Singh, N.; Kramer, S.; Stucky, G. D.; Moskovits, M. An Autonomous Photosynthetic Device in Which All Charge Carriers Derive from Surface Plasmons. *Nat. Nanotechnol.* **2013**, *8*, 247-251.

(45) Mubeen, S.; Lee, J.; Liu, D.; Stucky, G. D.; Moskovits, M. Panchromatic Photoproduction of H_2 with Surface Plasmons. *Nano Lett.* **2015**, *15*, 2132-2136.

(46) Tian, Y.; Tatsuma, T. Mechanisms and Applications of Plasmon-Induced Charge Separation at TiO_2 Films Loaded with Gold Nanoparticles. *J. Am. Chem. Soc.* **2005**, *127*, 7632-7637.

(47) DuChene, J. S.; Sweeny, B. C.; Johnston-Peck, A. C.; Su, D.; Stach, E. A.; Wei, W. D. Prolonged Hot Electron Dynamics in Plasmonic-Metal/Semiconductor Heterostructures with Implications for Solar Photocatalysis. *Angew. Chem. Int. Ed.* **2014**, *53*, 7887-7891.

(48) Pu, Y.-C.; Wang, G.; Chang, K.-D.; Ling, Y.; Lin, Y.-K.; Fitzmorris, B. C.; Liu, C.-M.; Lu, X.; Tong, Y.; Zhang, J. Z.; Hsu, Y.-J.; Li, Y. Au Nanostructure-Decorated TiO_2 Nanowires Exhibiting Photoactivity Across Entire UV-visible Region for Photoelectrochemical Water Splitting. *Nano Lett.* **2013**, *13*, 3817-3823.

(49) Qian, K.; Sweeny, B. C.; Johnston-Peck, A. C.; Niu, W.; Graham, J. O.; DuChene, D. J.; Qiu, J.; Wang, Y.-C.; Engelhard, M. E.; Su, D.; Stach, E. A.; Wei, W. D. Surface Plasmon-Driven Water Reduction: Gold Nanoparticle Size Matters. *J. Am. Chem. Soc.* **2014**, *136*, 9842-9845.

(50) Schlather, A. E.; Manjavacas, A.; Lauchner, A.; Marangoni, V. S.; DeSantis, C. J.; Nordlander, P.; Halas, N. J. Hot Hole Photoelectrochemistry on Au@SiO_2@Au Nanoparticles. *J. Phys. Chem. Lett.* **2017**, *8*, 2060-2067.

(51) Zhao, J.; Nguyen, S. C.; Ye, R.; Ye, B.; Weller, H.; Somorjai, G. A.; Alivisatos, A. P.; Toste, F. D. A Comparison of Photocatalytic Activities of Gold Nanoparticles Following Plasmonic and Interband Excitation and a Strategy for Harnessing Interband Hot Carriers for Solution Phase Photocatalysis. *ACS Cent. Sci.* **2017**, *3*, 482-488.

(52) Al-Zubeidi, A.; Hoener, B. S.; Collins, S. S. E.; Wang, W.; Kirchner, S. R.; Jebeli, S. A. H.; Joplin, A.; Chang, W.-S.; Link, S.; Landes, C. F. Hot Holes Assist Plasmonic Nanoelectrode Dissolution. *Nano Lett.* **2019**, *19*, 1301-1306.

(53) Yu, W.; Wijesekara, K. D.; Xi, X.; Willets, K. A. Quantifying Wavelength-Dependent Plasmonic Hot Carrier Energy Distributions at Metal/Semiconductor Interfaces. *ACS Nano* **2019**, *13*, 3629-3637.

(54) Pensa, E.; Garguilo, J.; Lauir, A.; Schlucker, S.; Cortes, A.; Maier, S. A. Spectral Screening of the Energy of Hot Holes over a Particle Plasmon Resonance. *Nano Lett.* **2019**, *19*, 1867-1874.

(55) Matsui, T.; Li, Y.; Hsu, M.-H. M.; Merckling, C.; Oulton, R. F.; Cohen, L. F.; Maier, S. A. Highly Stable Plasmon Induced Hot Hole Transfer into Silicon via a $SrTiO_3$ Passivation Interface. *Adv. Fun. Mater.* **2018**, *28*, 1705829.

(56) Güsken, N. A.; Lauri, A. Li, Y.; Matsui, T.; Doiron, B.; Bower, R.; Regoutz, A.; Mihai, A.; Petrov, P. K.; Oulton, R. F.; Cohen, L. F.; Maier, S. A. TiO_{2-x}-Enhanced IR Hot Carrier Based Photodetection in Metal Thin Film–Si Junctions. *ACS Photon.* **2019**, *6*, 953-960.

(57) Tanzid, M.; Ahmadivand, A.; Zhang, R.; Cerjan, B.; Sobhani, A.; Yazdi, S.; Nordlander, P.; Halas, N. J. Combining Plasmonic Hot Carrier Generation with Free Carrier Absorption for High-Performance Near-Infrared Silicon-Based Photodetection. *ACS Photon.* **2018**, *5*, 3472-3477.

(58) Cai, Y.-Y.; Collings, S. S. E.; Gallagher, M. J.; Bhattacharjee, U.; Zhang, R.; Chow, T. H.; Ahmadivand, A.; Ostovar, B.; Al-Zubeidi, A.; Wang, J.; Nordlander, P.; Landes, C. F.; Link, S. Single-Particle Emission Spectroscopy Resolves d-Hole Relaxation in Copper Nanocubes. *ACS Energy Lett.* **2019**, *4*, 2458-2465.

(59) He, J.; Lindström, E.; Hagfeldt, A.; Lindquist, S.-E. Dye-Sensitized Nanostructured p-Type Nickel Oxide Film as a Photocathode for a Solar Cell. *J. Phys. Chem. B* **1999**, *103*, 8940-8943.

(60) Irwin, M. D.; Buchholz, D. B.; Hains, A. W.; Chang, R. P. H.; Marks, T. J. *p*-Type Semiconducting Nickel Oxide as an Efficiency-Enhancing Anode Interfacial Layer in Polymer Bulk-Heterojunction Solar Cells. *Proc. Natl. Acad. Sci.* **2008**, *105*, 2783-2787.

(61) Seo, S.; Park, I. J.; Kim, M.; Lee, S.; B. C.; Jung, H. S.; Park, N.-G.; Kim, J. Y.; Shin, H. An Ultra-Thin, Un-Doped NiO Hole Transporting Layer of Highly Efficient (16.4%) Organic–Inorganic Hybrid Perovskite Solar Cells. *Nanoscale* **2016**, *8*, 11403.

(62) Kamata, R.; Kumagai, H.; Yamazaki, Y.; Sahara, G.; Ishitani, O. Photoelectrochemical CO_2 Reduction Using a Ru(II)-Re(I) Supramolecular Photocatalyst Connected to a Vinyl Polymer on a NiO Electrode. *ACS Appl. Mater. Interfaces* **2019**, *11*, 5632-5641.

(63) Thimsen, E.; Martinson, A. B. F.; Elam, J. W.; Pellin, M. J. Energy Levels, Electronic Properties, and Rectification in Ultrathin p-NiO Films Synthesized by Atomic Layer Deposition. *J. Phys. Chem. C* **2012**, *116*, 16830-16840.

(64) Guatam, G. S.; Senftle, T. P.; Alidoust, N.; Carter, E. A. Novel Solar Cell Materials: Insights from First-Principles. *J. Phys. Chem. C* **2018**, *122*, 27107-27126.

(65) Robatjazi, H.; Bahauddin, S. M.; Doiron, C.; Thomann, I. Direct Plasmon-Driven Photoelectrocatalysis. *Nano Lett.* **2015**, *15*, 6155-6161.

(66) Nakamura, K.; Oshikiri, T.; Ueno, K.; Wang, Y.; Kamta, Y.; Kotake, Y.; Misawa, H. Plasmon-Enhanced Photocurrent Generation and Water Oxidation with a Gold Nanoisland-Loaded Titanium Dioxide Photoelectrode. *J. Phys. Chem. Lett.* **2015**, *7*, 1004-1009.

(67) Kao, K.-C.; Kuroiwa, Y.; Nishi, H.; Tatsuma, T. Hydrogen Evolution from Water Based on Plasmon-Induced Charge Separation at a TiO_2/Au/NiO/Pt System. *Phys. Chem. Chem. Phys.* **2017**, *19*, 31429-31435.

(68) Anderson, P. A. The Work Function of Copper. *Phys. Rev.* **1949**, *76*, 388-390.

(69) Dabera, G. D. M. R.; Walker, M.; Sanchez, A. M.; Pereira, H. J.; Beanland, R.; Hatton, R. A. Retarding Oxidation of Copper Nanoparticles Without Electrical Isolation and the Size Dependence of Work Function. *Nat. Commun.* **2017**, *8*, 1894.

(70) Méndez-Medrano, M. G.; Kowalska, E.; Lehoux, A.; Herrisan, A.; Othani, B.; Bahena, D.; Briois, V.; Colbeau-Justin, C.; Rodríguez-López, J. L.; Remita, H. Surface Modification of TiO_2 with Ag Nanoparticles and CuO Nanoclusters for Application in Photocatalysis. *J. Phys. Chem. C* **2016**, *120,* 5143-5154.

(71) Yu, J.; Zhuang, S.; Xu, X.; Zhu, W.; Feng, B.; Hu, J. Photogenerated Electron Reservoir in Hetero-p–n CuO–ZnO Nanocomposite Device for Visible-Light-Driven Photocatalytic Reduction of Aqueous Cr(VI). *J. Mater. Chem. A* **2015**, *3*, 1199-1207.

(72) Scott, S. B.; Hogg, T. V.; Landers, A. T.; Maagaard, T.; Bertheussen, E.; Lin, J. C.; Davis, R. C.; Beeman, J. W.; Higgins, D.; Drisdell, W. S.; Hahn, C.; Mehta, A.; Seger, B.;

Jaramillo, T. F.; Chorkendorff, I. Absence of Oxidized Phases in Cu under CO Reduction Conditions. *ACS Energy Lett.* **2019**, *4*, 803-804.

(73) Corson, E. R.; Creel, E. B.; Kim, Y.; Urban, J. J.; Kostecki, R.; McCloskey, B. D. A Temperature-Controlled Photoelectrochemical Cell for Quantitative Product Analysis. *Rev. Sci. Instrum.* **2018**, *89*, 055112.

(74) Mukherjee, S.; Zhou, L.; Goodman, A. M.; Large, N.; Ayala-Orozco, C.; Zhang, Y.; Nordlander, P.; Halas, N. J. Hot-Electron-Induced Dissociation of H_2 on Gold Nanoparticles Supported on SiO_2. *J. Am. Chem. Soc.* **2014**, *136,* 64-67.

(75) Zhou, L.; Zhang, C.; McClain, M. J.; Manjavacas, A.; Krauter, C. M.; Shu, T.; Berg, F.; Everitt, H. O.; Carter, E. A.; Nordlander, P.; Halas, N. J. Aluminum Nanocrystals as a Plasmonic Photocatalyst for Hydrogen Dissociation. *Nano Lett.* **2016**, *16*, 1478-1484.

(76) Zhang, C.; Zhao, H.; Zhou, L.; Schlather, A. E.; Dong, L.; McClain, M. J.; Swearer, D. F.; Nordlander, P.; Halas, N. J. Al–Pd Nanodisk Heterodimers as Antenna–Reactor Photocatalysts. *Nano Lett.* **2016**, *16*, 6677-6682.

(77) Nørskov, J. K.; Abild-Pedersen, F.; Studt, F.; Bligaard, T. Density Functional Theory in Surface Chemistry and Catalysis. *Proc. Natl. Acad. Sci.* **2011**, *108*, 937-943.

(78) Hammer, B.; Nørskov, J. K. Theoretical Surface Science and Catalysis—Calculations and Concepts. *Adv. Catal.* **2000**, *45*, 71-129.

(79) Sundararaman, R.; Narang, P.; Jermyn, A. S.; Goddard III, W. A.; Atwater, H. A. Theoretical Predictions for Hot-Carrier Generation from Surface Plasmon Decay. *Nat. Commun.* **2014**, *5*, 5788.

(80) Brown, A. M.; Sundararaman, R.; Narang, P.; Goddard III, W. A.; Atwater, H. A. Nonradiative Plasmon Decay and Hot Carrier Dynamics: Effects of Phonons, Surfaces, and Geometry. *ACS Nano* **2016**, *10*, 957-966.

(81) Wuttig, A.; Yaguchi, M.; Motobayashi, K.; Osawa, M.; Surendranath, Y. Inhibited Proton Transfer Enhances Au-Catalyzed CO_2-to-Fuels Selectivity. *Proc. Natl. Acad. Sci.* **2016**, *113*, E4585-E4593.

(82) Christopher, P.; Xin, H.; Marimuthu, A.; Linic, S. Singular Characteristics and Unique Chemical Bond Activation Mechanisms of Photocatalytic Reactions on Plasmonic Nanostructures. *Nat. Mater.* **2012**, *11*, 1044-1050.

(83) Boerigter, C.; Campana, R.; Morabito, M.; Linic, S. Evidence and Implications of Direct Charge Excitation as the Dominant Mechanism in Plasmon-Mediated Photocatalysis. *Nat. Commun.* **2016**, *7*, 10545.

(84) Boerigter, C.; Aslam, U.; Linic, S. Mechanism of Charge Transfer from Plasmonic Nanostructures to Chemically Attached Materials. *ACS Nano*, **2016**, *10*, 6108-6115.

(85) Rao, V. G.; Aslam, U.; Linic, S. Chemical Requirement for Extracting Energetic Charge Carriers from Plasmonic Metal Nanoparticles to Perform Electron-Transfer Reactions. *J. Am. Chem. Soc.* **2019**, *141,* 643-647.

(86) Aslam, U.; Rao, V. G.; Chavez, S.; Linic, S. Catalytic Conversion of Solar to Chemical Energy on Plasmonic Metal Nanostructures. *Nat. Catal.* **2018**, *1*, 656-665.

(87) Wu, K.; Chen, J.; McBride, J. R.; Lian, T. Efficient Hot-Electron Transfer by a Plasmon-Induced Interfacial Charge-Transfer Transition. *Science* **2015**, *349*, 632-635.

(88) Tan, S. Argondizzo, A.; Ren, J.; Liu, L.; Zhao, J.; Petek, H. Plasmonic Coupling at a Metal/Semiconductor Interface. *Nat. Photon.* **2017**, *11*, 806-812.

(89) Kumar, P. V.; Rossi, T. P.; Marti-Dafcik, D; Reichmuth, D.; Kuisma, M.; Erhart, P.; Puska, M. J.; Norris, D. J. Plasmon-Induced Direct Hot-Carrier Transfer at Metal–Acceptor Interfaces. *ACS Nano* **2019**, *13*, 3188-3195.

(90) Zhang, Y.; Nelson, T.; Tretiak, S.; Guo, H.; Schatz, G. C. Plasmonic Hot-Carrier-Mediated Tunable Photochemical Reactions. *ACS Nano* **2018**, *12*, 8415-8422.

Table of Contents Image